

Anisotropic Particles Focusing Effect in Complex Flows

S  verine Atis,^{1,2} Matthieu Leclair,¹ Themistoklis Sapsis,¹ and Thomas Peacock¹

¹*Massachusetts Institute of Technology, Department of Mechanical Engineering, Cambridge, Massachusetts 02139.*

²*University of Chicago, Department of Physics, Chicago, Illinois 60637*

The dispersion of a tracer in a fluid flow is influenced by the Lagrangian motion of fluid elements. Even in laminar regimes, the irregular chaotic behavior of a fluid flow can lead to effective stirring that rapidly redistributes a tracer throughout the domain. When the advected particles possess a finite size and nontrivial shape, however, their dynamics can differ markedly from passive tracers, thus affecting the dispersion phenomena. Here we investigate the behavior of neutrally buoyant particles in 2-dimensional chaotic flows, combining numerical simulations and laboratory experiments. We show that depending on the particles shape and size, the underlying Lagrangian coherent structures can be altered, resulting in distinct dispersion phenomena within the same flow field. Experiments performed in a two-dimensional cellular flow, exhibited a focusing effect in vortex cores of particles with anisotropic shape. In agreement with our numerical model, neutrally buoyant ellipsoidal particles display markedly different trajectories and overall organization than spherical particles, with a clustering in vortices that changes accordingly with the aspect ratio of the particles.

February 28, 2025

The dynamics of finite-size particles in fluid flows can be considerably different from infinitesimal fluid particles, leading to distinct clustering and dispersion phenomena. From pollutant transport and plankton distribution on the ocean surface, to accretion phenomena in astrophysics, predicting the dynamics of finite-sized objects in a given field of force matters in a wide variety of natural phenomena and industrial processes. The repercussions of finite-size effects on the transport of material particles are crucial in understanding many geophysical and environmental processes, as well as for ocean decision-making strategies, and presses the need for improved predictive capability of material dispersion in fluid flows.

In this context, Lagrangian coherent structures (LCS) provide a useful framework to understand the transport of material in complex, unsteady flow fields [1]. However, depending on their size and buoyancy, objects that present inertia can follow markedly different trajectories than passive fluid particles [2–4]. The shape of the particles; i.e their symmetry properties, can also affect their response to fluid flows, leading to distinct behaviors between anisotropic objects and their symmetric counterpart [5, 6]. For instance, in cloud formation process, the anisotropic shape of ice particles influences their transport [6] and aggregation [7, 8] in turbulent atmospheric flows. Fiber transport in cellular flows, on the other hand, can lead to very different hydrodynamic dispersion depending on the buckling properties of the material [9, 10]. Under marine conditions on the other hand, preferential alignment of elongated microorganisms in the flow local direction can also change the light backscattering and alter the rates of global carbon fixation in phytoplankton blooms [11]. In recent studies, predictive models suggested that the irregular shape of microplastic contaminants can influence the long term transport on the surface of the ocean [12–14].

In this paper, we investigate experimentally the long term dynamics of rod shape particles with various aspect

ratio, in a quasi-2-dimensional Stokes flow. We present a simple model that combines finite-size effects with an orientational-dependent dynamics, and perform in parallel, numerical simulations under identical conditions to the experiments. Our results suggest that particles with anisotropic shape present stronger inertial effects than spherical particles, and are attracted to regions with higher vorticity.

Inertial effects arise when the advected particle’s acceleration is different from the carrier fluid’s acceleration; namely, the particles are responding to changes in the underlying flow field over a finite time, for instance when the density of the advected particles and the density of the fluid are different. Even for small density differences, these effects can accumulate over time and eventually lead the particles to exhibit drastic deviations from the fluid flow trajectories. To account for these additional forces, the particles dynamics can be described by the Maxey-Riley equation [15, 16]. Assuming the particle’s radius a is much smaller than the characteristic flow length scale L , the Fax  n correction terms and the memory term can be neglected, and after rescaling space by L , and time by $T = L/U$, with U the characteristic flow velocity, the simplified equation of motion becomes [17]:

$$\frac{d\mathbf{v}}{dt} = \frac{3R}{2} \frac{D\mathbf{u}}{Dt} - \frac{R}{St}(\mathbf{v} - \mathbf{u}) + \left(1 - \frac{3R}{2}\right) \mathbf{g}. \quad (1)$$

The particle’s velocity \mathbf{v} variation now depends on three forces described by the right hand side of the equation. The first term accounts for advection and added mass, with \mathbf{u} the flow velocity, the second one is the Stokes drag force, and the third is the buoyancy force, where \mathbf{g} is gravity. Note that $d./dt = \frac{\partial}{\partial t} + (\mathbf{v} \cdot \nabla)$. and $D./Dt$ are considered different here since the particles are neutrally buoyant but not infinitesimally small [18]. The difference between the particle density ρ_p and the fluid density ρ_f is characterize by the ratio $R = 2\rho_f/(\rho_f + 2\rho_p)$, and St

is the particle's Stokes number, given by:

$$\text{St} = \frac{2}{9} \frac{\rho_p}{\rho_f} \left(\frac{a}{L}\right)^2 \text{Re}, \quad (2)$$

wheres $\text{Re} = UL/\nu$ is the flow Reynolds number and ν the fluid kinematic viscosity. This simplified Maxey-Riley equation has been commonly used in the literature to describe small but finite-size particle's dynamics [2, 16–19]. For instance, experiments conducted in 3-dimensional turbulent flows [4, 20–23], and in 2-dimensional chaotic flow [3, 18], have shown that the particles behavior can be partly quantified by the particle's Stokes number.

When the particles are neutrally buoyant, such that $\rho_p = \rho_f$, the equation (1) converges toward the fluid elements motion for infinitesimal particles $a \ll L$, such that $\text{St} \rightarrow 0$. However, if the particle's size is not negligible, their dynamics can exhibit a finite relaxation time due to the interactions of the flow over the particle's surface [2–4, 18]. Even for neutrally buoyant particles, these effects can be responsible for additional forces acting on the particle, and can result as well in particles' trajectories to deviate from the fluid flow. For neutrally buoyant particles $R = 2/3$, and equation (1) becomes [17]:

$$\frac{d\mathbf{v}}{dt} = \frac{D\mathbf{u}}{Dt} - \frac{2}{3}\text{St}^{-1}(\mathbf{v} - \mathbf{u}). \quad (3)$$

Compared with spheres, non-spherical particles exhibit an additional mechanisms due to the coupling between translational and rotational behavior. These particles can then experience both a torque and an orientation dependent drag force. The motion of small, neutrally buoyant ellipsoidal particles in laminar flow has been first studied by G. B. Jeffery in 1922 [24]. His theoretical work on the torque experienced by non-inertial ellipsoidal particles, and more recently, numerical simulations on anisotropic particles undergoing orientation dependent drag force and relaxation times [5, 14, 25], suggest that the dynamics of even very small objects, i. e. $\text{St} \ll 1$, can be strongly modified due to their shape. Experiments in turbulent flow, have also indicated that the turbulent kinetic energy of a suspension is altered accordingly with the suspended particles' shape [26]. Finally, even with weak inertial effects coupled with orientation dependent forces, the transport of anisotropic particles can lead to distinct trajectories over long period of times [14].

Model

To describe the effects resulting from finite size and anisotropic shape with a minimal model, we present here an equation of motion that couples the particle's orientation with the drag force. Neutrally buoyant ellipsoidal particles experience a torque that tends to align their axes parallel to the surrounding fluid principal axis of distortion. When the particle's Reynolds number is negligible $\text{Re}_p = av/\nu \ll 1$, they can be considered iner-

tial and their velocity are equal to the surrounding fluid $\mathbf{v} = \mathbf{u}$ at all time, such that there is no resultant force acting on the particle [24]. In laminar flow, this resultant torque on the particle vanishes at first order, and the particle angular velocity $\dot{\theta}$ can be simply expressed as a function of the flow vorticity ω and strain-rate: [16, 24, 27, 28]:

$$\dot{\theta} = \frac{\omega}{2} + \frac{1}{2} \left(\frac{1 - \epsilon^2}{\epsilon^2 + 1} \right) \times \left[\sin 2\theta \left(\frac{\partial u_x}{\partial x} - \frac{\partial u_y}{\partial y} \right) - \cos 2\theta \left(\frac{\partial u_y}{\partial x} + \frac{\partial u_x}{\partial y} \right) \right] \quad (4)$$

where $\epsilon = b/a$ is the particle aspect ratio, with a and b the semi-minor and semi-major axis respectively. In this configuration θ represent the angle of the particle major axis with $\hat{\mathbf{x}}$ in the fixed frame, and u_x and u_y are the horizontal and vertical components of the flow velocity in the same reference frame.

In order to consider finite-size particles, we need to take into account inertial forces that will tend to separate the particles trajectory from the fluid trajectory, such that now $\mathbf{v} \neq \mathbf{u}$. The dynamics of elongated particles is not well approximated by Eq. (3), and need to take into account orientation specific dynamics [29, 30]. For instance, the added mass and drag force terms can become dependent on the particle's instantaneous orientation [5, 14, 25]. Here, we present a linear momentum equation with a the hydrodynamic drag force term coupled with the particle's orientation [16, 31–34]:

$$\mathbf{F} = -6\pi a\mu \hat{\mathbf{K}}(\mathbf{v} - \mathbf{u}), \quad (5)$$

where μ is the dynamic viscosity of the fluid, and $\hat{\mathbf{K}}$ represents the resistance tensor of an ellipsoidal particle in the co-moving frame [5, 16, 33]. The resistance tensor $\hat{\mathbf{K}}$ is initially determined in the particle frame, and relates to $\hat{\mathbf{K}}$ in the co-moving frame through the particle rotation matrix \mathbf{A} :

$$\hat{\mathbf{K}} = \mathbf{A}^{-1} \hat{\mathbf{K}} \mathbf{A}. \quad (6)$$

In the case of a prolate ellipsoidal particle, e.g. invariant by rotation along its major axis, the resistance tensor reduces to a diagonal matrix. We note $\hat{\mathbf{K}} = 8/3\epsilon^{-1/3}\hat{\mathbf{k}}$ and two-dimensional flow, we have:

$$\hat{\mathbf{k}} = \begin{pmatrix} \frac{\epsilon^2 - 1}{\sqrt{\epsilon^2 - 1} \ln(\epsilon + \sqrt{\epsilon^2 - 1}) - \epsilon} & 0 \\ 0 & \frac{\epsilon^2 - 1}{\sqrt{\epsilon^2 - 1} \ln(\epsilon + \sqrt{\epsilon^2 - 1}) + \epsilon} \end{pmatrix}. \quad (7)$$

Substituting the drag force term applying to spheres in equation (3), we obtain:

$$\frac{d\mathbf{v}}{dt} = \frac{D\mathbf{u}}{Dt} - \frac{16}{9}(\epsilon\text{St})^{-1} \hat{\mathbf{k}}(\mathbf{v} - \mathbf{u}), \quad (8)$$

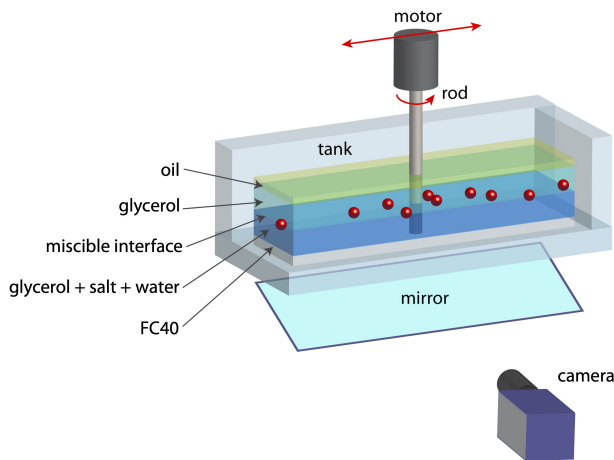


FIG. 1. Experimental setup of the rotor-oscillator flow: one rotor attached to a traverse, are respectively ensuring the rotation and translation of the rod. A mirror at 45 degrees is reflecting the recorded image of the interface from the bottom of the tank. The particles are trapped at the center of a stratified glycerol layer.

such that now, the equation of motion becomes coupled to the orientation of the particle given by Eq.(4) [16]. Note that the drag force term's prefactor is now proportional to $(\epsilon St)^{-1}$, and indicates that the relaxation time of the particle will now also depend on its aspect ratio; i.e. the more elongated the particle the longer the response time.

Methods

The experimental setup consists in a rectangular container of dimensions $L \times W \times h = 100 \times 400 \times 200$ mm. To circumvent any surface tension effect [36], the particles are trapped at the interface between two miscible fluids of different density. The tank is filled with two stratified layers of pure glycerol of density $\rho_1 = 1.26 \pm 0.001$ g.cm⁻³ and a solution of salted glycerol and 4% water of density $\rho_2 = 1.30 \pm 0.01$ g.cm⁻³, as represented in Fig. 1. In order to prevent any viscous instability at the interface, the viscosity of the salted layer is matched with pure glycerol by adding water. Viscosity measurements were performed with an Aton Paar MCR rheometer for different concentrations of water to adjust the viscosity of the salted glycerol solutions. Particles of density $\rho_p = 1.28 \pm 0.005$ are then trapped at the miscible interface leading to a quasi-2-dimensional layer of particle suspension. The bottom of the tank is filled with a 1 cm layer of FC-40 to reduce the friction at the bottom of the tank and a layer of vegetable oil on the top to prevent water absorption by the glycerol. The experiment is lighted from the top with a series of led and the particles motion is recorded with a 45 degree tilted mirror at the bottom the setup. Images are digitized with a 14 bit LaVision camera and particles tracking velocimetry (PTV) is performed from filtered images. 3d-printing ABS filament of 1.75 mm diameter was cut to different length to create

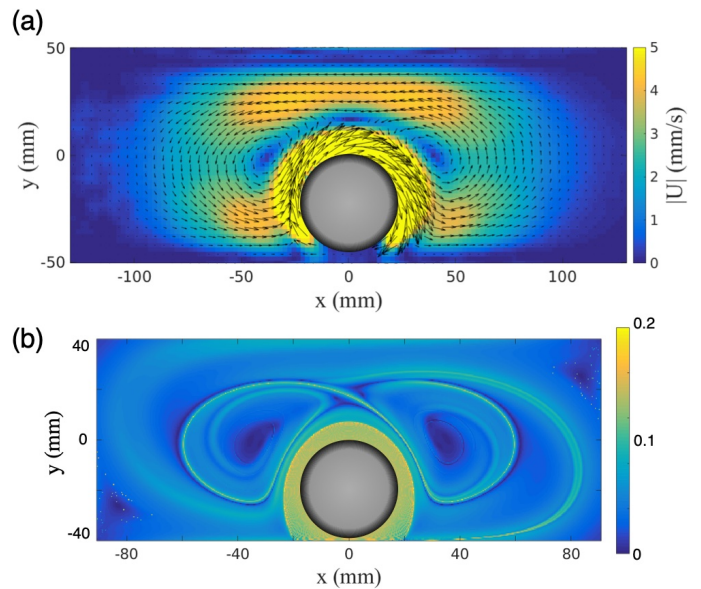


FIG. 2. (a) Experimental flow velocity field determined from PIV measurements, with a rotor speed at 100 rpm in a steady transversal position. The color code corresponds to the norm of the flow velocity. (b) Finite time Lyapunov exponent field determined from the analytical approximation of the rotor-oscillator flow [35].

anisotropic particles with the desired aspect ratios. To minimize particle-particle interactions, a small number of particles (32) is initially uniformly deposited across the domain. For each particle's aspect ratio, five independent realizations were prepared manually by randomly redistributing the initial positions of the particles at the glycerol/glycerol-and-salt interface, as shown in the supplemental figure [16]. Because of the stable stratification configuration and the high viscosity of the glycerol, the interface remains well define during consecutive realizations of the same experiment. The stratification is then renewed by changing the fluid mixture in the tank, and different particles are deposited at the interface.

The experimental flow is created by stirring the fluid with a rotating rod attached to a longitudinal translation stage. The rotation is controlled with a Lexium NEMA 34 motion control motor with a Plexiglas rod of 2 cm diameter, and the translation of the rotor with a Parker lead-screw traverse above the tank. The resulting flow is quasi-2-dimensional in the stratified fluid layer, and similar to the topology of the rotor-oscillator flow described by Hackborn [37]. In the steady regime, when the position of the rod is fixed, the rotation of the rod in the central region close to the bottom boundary creates a sequence of two Moffatt eddies [38] and a hyperbolic stagnation point in the center. Particle image velocimetry (PIV) is performed by seeding the upper glycerol layer

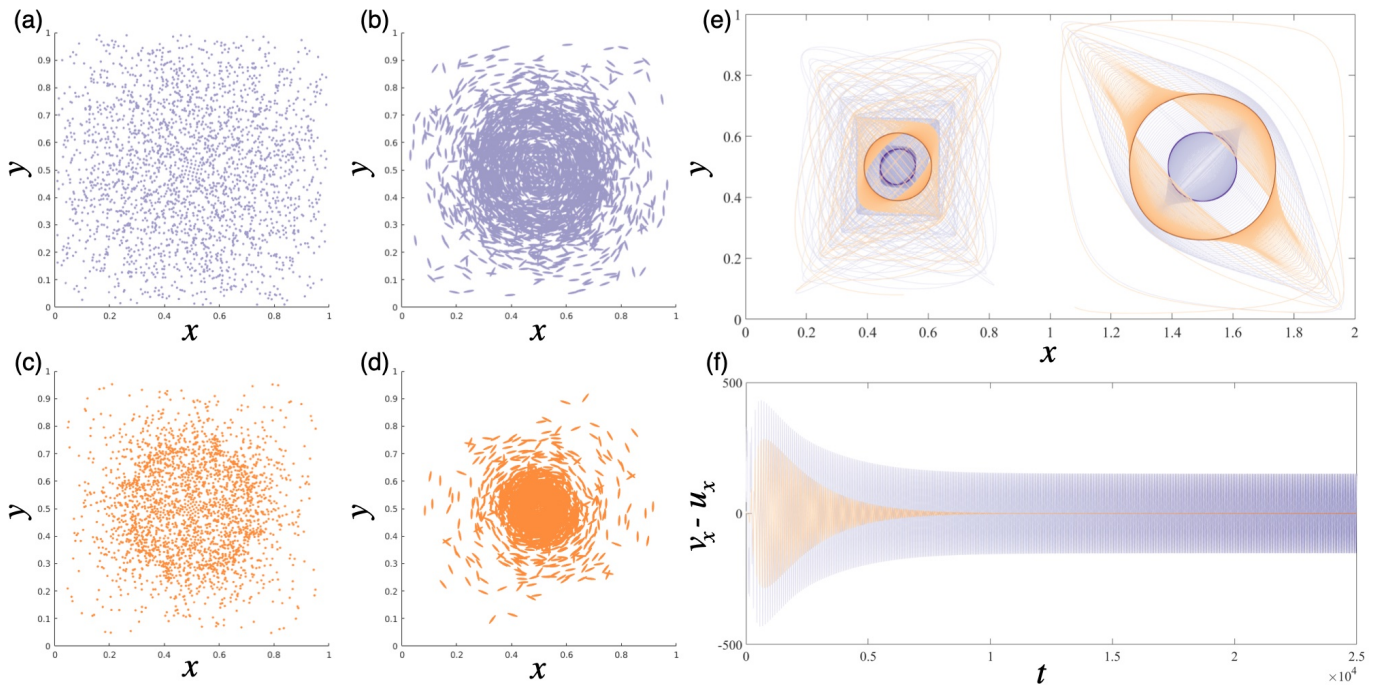


FIG. 3. Numerical particles positions after a transient regime in the steady vortex flow with $A = 100$ and $\omega = 2\pi/10$. For particles initially at rest and Stokes number $St = 5 \cdot 10^{-4}$ (a) spheres and (b) ellipsoids with $\epsilon = 5$, and $St = 10^{-3}$ (c) spheres and (d) ellipsoids with $\epsilon = 5$. (e) Trajectories for two spherical (orange) and two ellipsoidal (purple) particles with $St = 10^{-1}$ starting from the same initial positions. (f) Velocity difference $v_x - u_x$ variation over time between the particle velocity and the fluid velocity at the particle's position, for a spherical (orange) and an ellipsoidal (purple) particle.

with $30 \mu\text{m}$ diameter hollow glass beads. A YAG laser 532 nm is used to illuminate a sheet in the horizontal plane to visualize the flow at the vicinity of the plane containing the inertial particles. A typical flow velocity obtained from the PIV analysis is displayed on the Figure 2. The inner region in the direct proximity of the rotor exhibits the highest velocities $\|u\| \gtrsim 10 \text{ mm.s}^{-1}$, and rapidly decays within a rotor radius away from the rotating boundary. The two co-rotating Moffatt eddies are also visible, with an average flow speed in the outer region of $u \simeq 4 \pm 1 \text{ mm.s}^{-1}$ in their vicinity.

We perform in parallel numerical simulations solving the governing equations (4) and (8) under identical conditions with the experiments. In order to couple the equations (4) and (8) with the experimentally measured flow field, the velocity field is nondimensionalized such that $x^* = x/L$ with $L = 100 \text{ mm}$ corresponding to the width of the tank, and $u^* = uT/L$, where L/T is the characteristic flow velocity estimated from the average flow in the outer region surrounding the vortices. The size and the aspect ratio of the particles are set by choosing identical Stokes number and ϵ with the experimental particles. The particles initial positions are on a grid and start with a slightly smaller initial velocity relative to the fluid velocity, such that $\mathbf{v}(t=0) = 0.9\mathbf{u}$ at the particle's initial position, and the initial orientation of the anisotropic particles θ_0 are randomly distributed.

Results

We first numerically investigate the effect of particles size and shape on their trajectories over a large range of Stokes number $10^{-4} \leq St \leq 10^{-1}$, and aspect ratio $1 \leq \epsilon \leq 10$. We consider a double gyre flow with periodic boundary conditions defined by the stream function

$$\psi(x, y, t) = A \sin[\pi f(x, t)] \sin(\pi y), \quad (9)$$

where A sets the flow amplitude, $f(x, t) = x + B(x^2 - 2) \sin \omega t$, and B sets the oscillation amplitude. In the steady regime $B = 0$, and the stream function reduces to $\psi(x, y) = A \sin(\pi x) \sin(\pi y)$, leading to a simple vortex flow. The resulting trajectories and spatial distribution of neutrally buoyant particles with different shapes are shown in Figure 3 for two different Stokes number and a stream function amplitude of $A = 100$. At this flow amplitude, the inertial particles are rapidly converging to a steady spatial distribution. As can be seen from the particles distribution in Fig. 3(a)-(d), both types of particles display a preferential concentration in the vicinity of the vortex core, which increases with the St number. In addition, ellipsoidal particles orientation aligns with the local flow streamlines, and systematically present a stronger focusing behavior, converging toward smaller orbits radii at equal St number with the spherical particles. This effect can be attributed to the reduced prefactor in the drag force term in Eq. (8) for anisotropic particles which results in an increasingly larger relaxation time with ϵ to

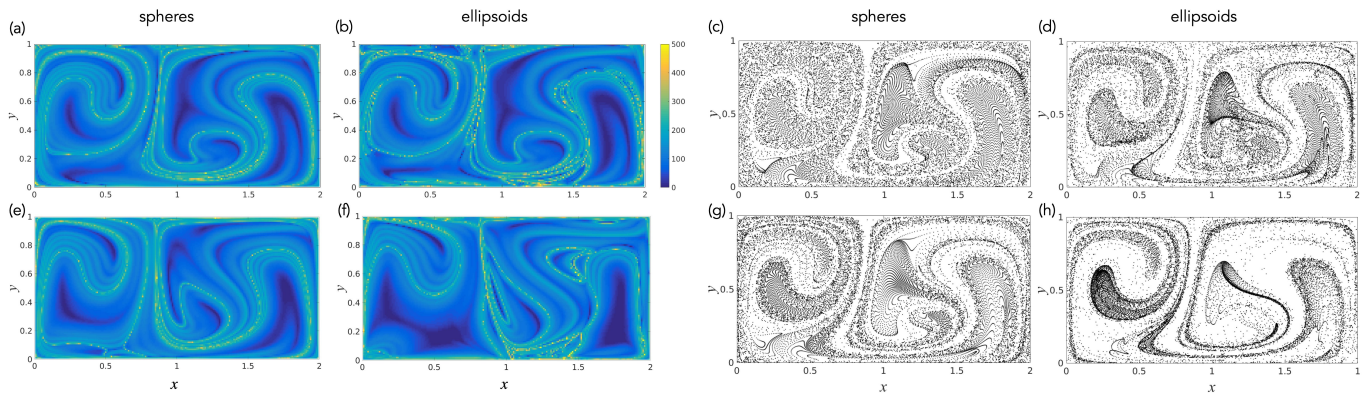


FIG. 4. Particles FTLE field in simulations with spherical particles, left column, and elliptical particles with $\epsilon = 5$, right column, after $T = 20$ time steps in a double-gyre flow. The corresponding flow parameters are: $A = 100$, $e = 0.25$, and $\omega = 2\pi A$ with a particle initial velocity at $\mathbf{v} = 0.9\mathbf{u}$, (a) and (b), and $\mathbf{v} = 0$, (e) and (f). Corresponding particles positions in simulations with spherical particles, left column, and elliptical particles with $\epsilon = 5$, right column

deviations from the flow velocity. Even at small St number $St \approx 10^{-4}$, when inertial effects are expected to be negligible, anisotropic particles' trajectories continues to exhibit a preferential concentration at a given distance from the vortex center, while spherical particles trajectories remain more uniformly distributed.

As can be seen in Figure 3(e) and (f), spherical particles with the largest simulated St numbers are rapidly trapped on a regular orbit, similar to the results show by Babiano et al. [18]. In contrast, anisotropic particles at equal St number exhibit a more irregular trajectory within the same flow field, the particle's velocity doesn't converge to the flow velocity field while their orbits are closer to the vortex core.

We now use the full time-dependent double gyre flow, and set $e = 0.25$. In time varying flows, attractive and repulsive structures are only defined over a finite-time window period. Regions with a low FTLE value is indicative of attractive properties; i.e. initially neighboring fluid particles remain close to each other over a given time window, while high values of the FTLE field correspond to repulsive regions of the flow, where the spatial separation over the same time window between neighboring fluid particles is maximized [1, 39]. Figures 4 compares spatial distribution and corresponding FTLE for spherical and ellipsoidal with two different St number and initial conditions. In all configurations, after $t = 2/A$, with $1/A$ corresponding to the gyre rotation period, the ellipsoidal particles distributions systematically present more contrasted spacial density variations than the spherical ones. The corresponding FTLE fields are then computed from the same finite-size particle trajectories [40]. While the spherical particles FTLE fields resemble the flow FTLE field (see the supp. mat. [16] for comparison) while the elliptical particles FTLE field are more affected and exhibit additional structures localized in regions with stronger mixing. This suggests that elliptical particles more complex dynamics lead to a de-

parture from passive particles dynamics in time varying flows even for very small St numbers.

We now present a series of experiments with rod shape particles for three different aspect ratio $\epsilon = 1, 2$ and 5 . The experimental flow has the geometry of a rotor-oscillator (RO) flow in the steady regime; an example of the flow velocity field is shown in Fig. 2(a) and more details can be found in [16]. We impose a constant rotor speed of 200 rpm for all the experiments. In this configuration, the Re number typically range between 10^{-1} and 10 over the flow field in the region away from the direct vicinity of the rotor. This leads to relatively small particle Stokes number $St \approx 10^{-4} - 10^{-3}$, such that, in the absence of anisotropy induced effects, we expect the particles to behave closer to tracers particles, and particles with $\epsilon = 1$ can be approximated with spherical particles. The particles are initially uniformly distributed across the experimental domain with no preferential alignment across the quasi-2-dimensional plane defined by the two-layer stratification, see [?] for details. Immediately after the flow is switched on, particles with $\epsilon > 1$ rotate along their \hat{z} axes and exhibit a preferential alignment of their principal axes with the local flow direction, as shown in the supplementary Figure [16] and supplemental movie 2. This suggests that the orientational behavior has a negligible response time to the changes in the flow field. The elongated particles almost instantaneously align with the local flow direction, in good agreement with our assumption in Eq. (4) and previous observations in flows at higher Reynolds number, where the particles align with the strongest Lagrangian stretching direction [28, 41]. The particles remain in the same plane for the entire duration of the experiments, and the principal axes of the elongated particles doesn't display off-plane motions except near the direct vicinity of the rotor.

After a time $t \gtrsim 6000\tau$, where $\tau = 0.3$ s corresponds to the rotor rotation time period, the particles spatial distribution approaches a stationary regime and exhibit a

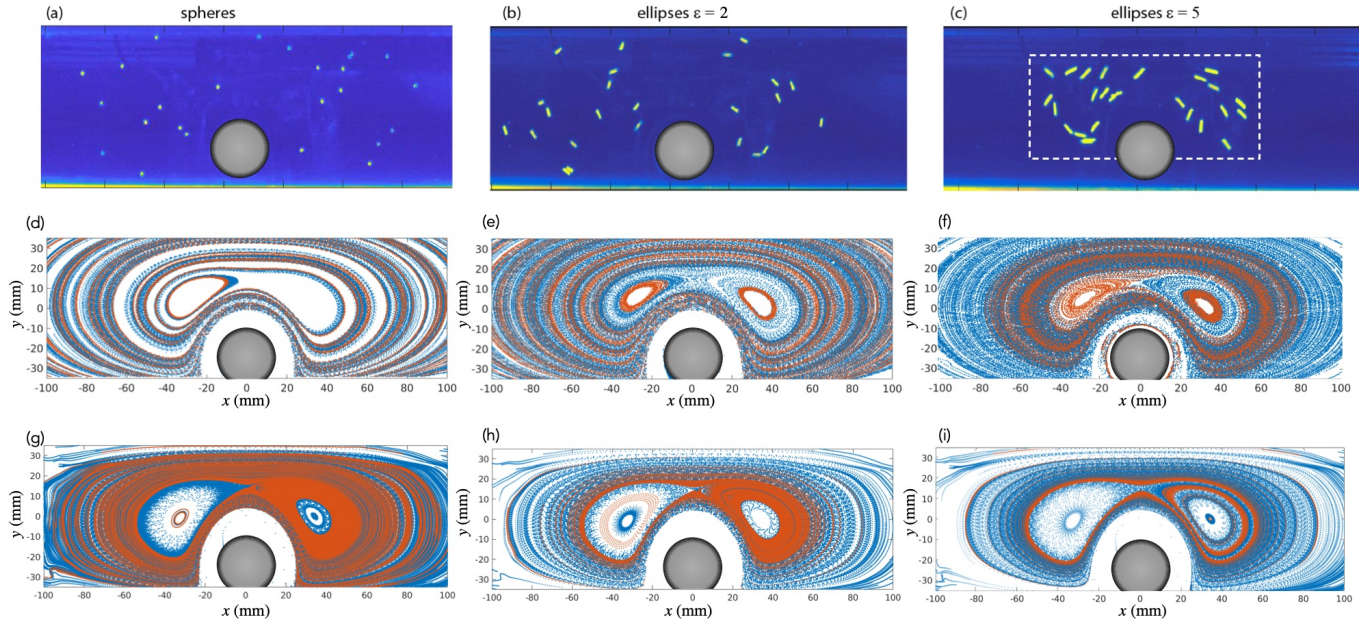


FIG. 5. Top row: experimental particles final positions at $t = 3500$ s, middle row: PTV determined from the corresponding experiments for $t = 0 - 3500$ s, bottom row: PTV determined from numerical particles trajectories coupled with the experimental flow field show in Fig. 2 for $t = 0 - 2000$ s.

strong dependence to aspect ratio, as can be seen on Fig. 5(a)-(c) and supplemental video 3. The final position of the particles with aspect ratio $\epsilon = 1$ do not exhibit any preferential concentration, and remain uniformly spread across the domain, while particles with $\epsilon = 2$ and $\epsilon = 5$ display a migration from the outer regions of the flow into the vortex cores and their vicinity. Remarkably, for $\epsilon = 5$, all the particles are focused in the central region. Note that for $\epsilon = 2$ and $\epsilon = 5$, a few particles can be attracted to the secondary vortices of the RO-flow near the edges of the tank and are not covered by our field of view in Fig. 2(a) and Fig. 5).

In order to quantify this behavior, we determine the individual particles trajectories using particle tracking velocimetry (PTV), and monitor their spatial distribution over time. Figure 5(d)-(f) displays the particles position as a function of time for the entire duration of the experiments corresponding to the snapshots in Figures 5(a)-(c) respectively. As can be seen in Fig. 5(e) and 5(f), in addition to be attracted to the central region of the flow field, some of the elongated particles' final trajectories form closed orbits inside the vortices. While for $\epsilon = 2$, the rest of the particles are evenly distributed in the vicinity the vortices, particles with $\epsilon = 5$ exhibit a strong concentration in a region encircling the two vortices. Figure 6 displays the measured particle density variation between $0 \leq t \leq 6000\tau$ in the central region of the flow shown by dashed white lines in Fig. 5(c). In a first transient regime, the spatial density of the elongated particles increases linearly over time with a larger migration rate for particles with larger aspect ratio ϵ . Af-

ter a time $t = t^*$, the migration ends and the density of particles in the central region of the flow remains constant over time. Interestingly, this saturation time scale $t^* \simeq 5000\tau = 1500$ s seems to be identical for both tested aspect ratio. On the other hand, particles with aspect ratio $\epsilon = 1$ present a negligible focusing effect, and their spatial distribution is stationary over time.

To test the accuracy of our model, we perform in parallel numerical simulations using the experimentally measured flow field shown in Fig. 2. The particles St number and aspect ratio are chosen identical to the experimental particles. The remaining free parameter, the characteristic time T of the flow field, is adjusted to give the best match between the experimental and numerical particles velocity for a given region of the flow, additional details can be found in the Methods section [16]. The best agreement with the experimental particles trajectories is obtained for a time scale of $T = 20$ s, and is in good agreement with the largest flow structure's average velocity $u = L/T \approx 5$ mm/s, as can be seen in Fig. 2(a). The resulting numerical trajectories are shown in Figure 5(g)-(i), and reproduce qualitatively the corresponding experimental trajectories. They present a similar convergence toward the vicinity of the vortices, although a larger asymmetry between the left and right attractive regions within the vortices is visible and only the right vortex traps the elongated particles on a distinct inner orbit. The migration dynamics of the numerical particles are shown in Fig. 6, and display a similar trend with the experiments. A short quantitative match of the particle density variation is obtained for $t \lesssim 500$ s, after

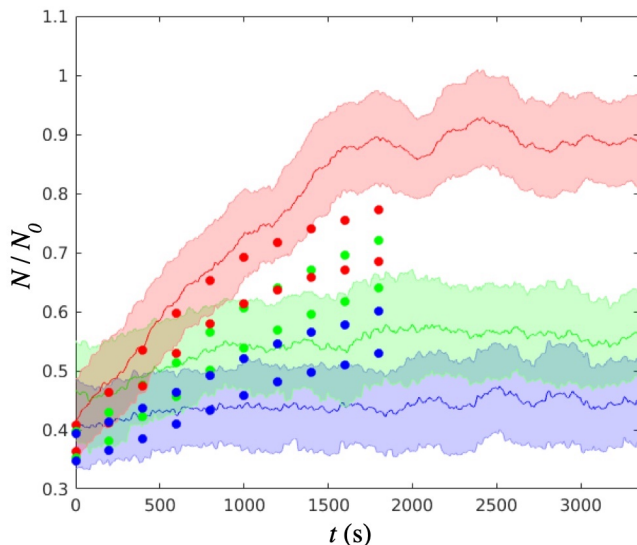


FIG. 6. Spatial particle density in variation as a function of time in the central region of the flow indicated by white dashed lines in Fig. 5c). Experimental data: lines represent average value and shaded region the error. Numerical particles with $St = 5 \cdot 10^{-4}$ coupled with the same experimental flow field: dots, the two series of data correspond to simulations with two different sets of parameters, see [16] for details. Blue : $\epsilon = 1$, green : $\epsilon = 2$, and red : $\epsilon = 5$

which the numerical particles start entering the saturation regime around $t \simeq 2500\tau = 750$ s, a little earlier than the experimental value $t^* \simeq 5000\tau$.

Comparing the shape of high particle concentration regions in the numerical simulations with the RO flow FTLE field shown in Fig ??(b), we can identify to which flow structures the particles are attracted to. The FTLE field displays several ridges. Two minima are created in the vortex cores, and correspond to the two elliptical regions where the elongated particles are trapped in the experiments. A third structure can be identify and corresponds to the minima of the FTLE field that forms a larger orbit encircling the two vortices. Both experimental and numerical particles with the largest aspect ratio $\epsilon = 5$ are specifically attracted to this region as can be seen in Fig 5f) and 5i).

Discussion

In our experiments, the observed migration toward vortices for elongated particles with a small Stokes number $St \sim 10^{-4}$, suggests that even weak deviations from passive trajectories can build up over time, and lead to dramatically different dynamics over long time periods.

These perturbations are not sufficient to significantly alter particles trajectories with an aspect ratio $\epsilon = 1$, and particles with $\epsilon = 2$ exhibit a significantly weaker focusing effect than those with $\epsilon = 5$. A direct comparison of these observations with numerical simulations, shows that our minimal model qualitatively describes this behavior, although the particles focusing effect exhibits a more moderate dependence to the particle aspect ratio ϵ than in the experiments. This difference could be attributed to second order orientation dependent terms, such as the added mass [5, 14, 25, 29, 30], that are neglected here.

These results suggest that anisotropic particles respond to the flow with a stronger lag, such that in Eq. 8 $St' = \epsilon St$ can be interpreted as an “effective” Stokes number St' that increases with ϵ . When the inertial effects are small, i. e. for smaller St number, the difference between St and St' becomes relevant only over larger time scales, such that small differences in the particles dynamics lead to distinct trajectories after a long time period. This effect could potentially enhance the migration rate of irregularly shaped microplastic toward gyres of marine debris [13, 14], and influence the garbage patches formation dynamics [12, 42]. On the opposite length and time scales, in biology this interplay between the shape of the particle and the flow field structures could influence the selective capture of microorganisms by larger animals. For instance, flows created by the beating of cilia can generate a local flow that attract only microorganisms of an optimal size [43]. Identical mechanisms could potentially select for an optimum shape, for instance, the aspect ratio of a given bacteria.

In conclusion, even neutrally buoyant particles with small particle Stokes number $St \simeq 10^{-4}$ exhibit trajectories that deviate from the fluid flow when they possess an anisotropic shape. Both experimental and numerical particles exhibit a migration toward the regions in the vicinity of the vortices. The orientational dependence of the drag term in our minimal model describes the particles dynamics qualitatively, suggesting that this effect might be sufficient to capture the separation between isotropic and anisotropic particles trajectories in cellular flows. In addition, the effect of other orientation dependent terms should be studied in future work.

Acknowledgements

The authors would like to thank A.W. Murray and E. Climent for stimulating discussions, G. Haller, T. Witten and E. Kanso for their interesting comments. S. Atis was supported by the French government DGA/DS - Mission pour la Recherche et l’Innovation Scientifique fellowship during her visit at MIT.

[1] Thomas Peacock and George Haller, “Lagrangian coherent structures The hidden skeleton of fluid flows,” *Physics Today* **66**, 41–47 (2013).

[2] George Haller and Themistoklis Sapsis, “Where do inertial particles go in fluid flows?” *Physica D-nonlinear Phenomena* **237**, 573–583 (2008).

- [3] Nicholas T Ouellette, P J J O'Malley, and J P Gollub, "Transport of Finite-Sized Particles in Chaotic Flow," *Physical Review Letters* **101**, 174504 (2008).
- [4] Rachel D Brown, Z Warhaft, and Greg A Voth, "Acceleration Statistics of Neutrally Buoyant Spherical Particles in Intense Turbulence," *Physical Review Letters* **103**, 194501 (2009).
- [5] H F Zhang, G Ahmadi, F G Fan, and J B McLaughlin, "Ellipsoidal particles transport and deposition in turbulent channel flows," *International Journal of Multiphase Flow* **27**, 971–1009 (2001).
- [6] Rui Ni, Nicholas T Ouellette, and Greg A Voth, "Alignment of vorticity and rods with Lagrangian fluid stretching in turbulence," *Journal of Fluid Mechanics* **743**, R3 (2014).
- [7] Ewe Wei Saw, Raymond A Shaw, Sathyanarayana Ayyalasomayajula, Patrick Y Chuang, and Armann Gylfason, "Inertial clustering of particles in high-reynolds-number turbulence," *Physical Review Letters* **100**, 214501 (2008).
- [8] K D SQUIRES and J K EATON, "Particle Response and Turbulence Modification In Isotropic Turbulence," *Physics of Fluids A-fluid Dynamics* **2**, 1191–1203 (1990).
- [9] Elie Wandersman, Nawal Quennouz, Marc Fermigier, Anke Lindner, and O Du Roure, "Buckled in translation," *Soft matter* **6**, 5715–5719 (2010).
- [10] N Quennouz, Michael Shelley, O Du Roure, and A Lindner, "Transport and buckling dynamics of an elastic fibre in a viscous cellular flow," *J Fluid Mech* **769**, 387–402 (2015).
- [11] Marcos, Justin R Seymour, Mitul Lohar, William M Durham, James G Mitchell, Andreas Macke, and Roman Stocker, "Microbial alignment in flow changes ocean light climate," *Proceedings of the National Academy of Sciences of the United States of America* **108**, 3860–3864 (2011).
- [12] C Broday, D and Fichman, M and Shapiro, M and Gutfinger, "Motion of diffusionless particles in vertical stagnation flows—II. Deposition efficiency of elongated particles," *Journal of Aerosol Science* **28**, 35–52 (1997).
- [13] I Chubarenko, A Bagaev, M Zobkov, and E Esiukova, "On some physical and dynamical properties of microplastic particles in marine environment," *MPB* **108**, 105–112 (2016).
- [14] Michelle H Dibenedetto, Nicholas T Ouellette, and Jeffrey R Koseff, "Transport of anisotropic particles under waves," , 320–340 (2018).
- [15] M R Maxey and J J Riley, "Equation of Motion For A Small Rigid Sphere In A Nonuniform Flow," *Physics of Fluids* **26**, 883–889 (1983).
- [16] Supplementary material, "No Title," .
- [17] Themistoklis P Sapsis, Nicholas T Ouellette, Jerry P Gollub, and George Haller, "Neutrally buoyant particle dynamics in fluid flows: Comparison of experiments with Lagrangian stochastic models," *Physics of Fluids* **23**, 93304 (2011).
- [18] Armando Babiano, Julyan H E Cartwright, Oreste Piro, and Antonello Provenzale, "Dynamics of a small neutrally buoyant sphere in a fluid and targeting in Hamiltonian systems," *Physical Review Letters* **84**, 5764 (2000).
- [19] E E Michaelides, "The Transient Equation of Motion for Particles, Bubbles, and Droplets," *Journal of fluids engineering* **119**, 233 (1997).
- [20] A La Porta, G A Voth, A M Crawford, J Alexander, and E Bodenschatz, "Fluid particle accelerations in fully developed turbulence," *Nature* **409**, 1017–1019 (2001).
- [21] R Volk, E Calzavarini, E Leveque, and J . F Pinton, "Dynamics of inertial particles in a turbulent von Karman flow," *Journal of Fluid Mechanics* **668**, 223–235 (2011).
- [22] Enrico Calzavarini, Romain Volk, Emmanuel Leveque, Jean-Francois Pinton, and Federico Toschi, "Impact of trailing wake drag on the statistical properties and dynamics of finite-sized particle in turbulence," *Physica D-nonlinear Phenomena* **241**, 237–244 (2012).
- [23] Simon Klein, Mathieu Gibert, Antoine Berut, and Eberhard Bodenschatz, "Simultaneous 3D measurement of the translation and rotation of finite-size particles and the flow field in a fully developed turbulent water flow," *Measurement Science & Technology* **24**, 24006 (2013).
- [24] G B Jeffery, "The motion of ellipsoidal particles in a viscous fluid," *Proceedings of the Royal Society of London Series A-containing Papers of A Mathematical and Physical Character* **102**, 161–179 (1922).
- [25] P H Mortensen, H I Andersson, J J J Gillissen, and B J Boersma, "Dynamics of prolate ellipsoidal particles in a turbulent channel flow," *Physics of Fluids* **20**, 93302 (2008).
- [26] Gabriele Bellani, Margaret L Byron, Audric G Collignon, Colin R Meyer, and Evan A Variano, "Shape effects on turbulent modulation by large nearly neutrally buoyant particles," *Journal of Fluid Mechanics* **712**, 41–60 (2012).
- [27] J A Olson and R J Kerekes, "The motion of fibres in turbulent flow," *Journal of Fluid Mechanics* **377**, 47–64 (1998).
- [28] Shima Parsa, Jeffrey S Guasto, Monica Kishore, Nicholas T Ouellette, J P Gollub, and Greg A Voth, "Rotation and alignment of rods in two-dimensional chaotic flow," *Physics of Fluids* **23**, 43302 (2011).
- [29] I Gallily and A H Cohen, "Orderly Nature of the Motion of Nonspherical Aerosol-particles .2. Inertial Collision Between A Spherical Large Droplet and An Axially Symmetrical Elongated Particle," *Journal of Colloid and Interface Science* **68**, 338–356 (1979).
- [30] D L Koch and E S G Shaqfeh, "The Instability of A Dispersion of Sedimenting Spheroids," *Journal of Fluid Mechanics* **209**, 521–542 (1989).
- [31] H Brenner, "The Stokes Resistance of An Arbitrary Particle .3. Shear Fields," *Chemical Engineering Science* **19**, 631–651 (1964).
- [32] H Brenner, "The Stokes Resistance of An Arbitrary Particle .4. Arbitrary Fields of Flow," *Chemical Engineering Science* **19**, 703–727 (1964).
- [33] Fa-Gung Fan and Goodarz Ahmadi, "Dispersion of ellipsoidal particles in an isotropic pseudo-turbulent flow field," *Journal of fluids engineering* **117**, 154–161 (1995).
- [34] E Loth, "Drag of non-spherical solid particles of regular and irregular shape," *Powder Technology* **182**, 342–353 (2008).
- [35] M Weldon, T Peacock, G B Jacobs, M Helu, and G Haller, "Experimental and numerical investigation of the kinematic theory of unsteady separation," *Journal of Fluid Mechanics* **611**, 1–11 (2008).
- [36] Dominic Vella and L Mahadevan, "The "Cheerios effect"," *American Journal of Physics* **73**, 817 (2005).
- [37] W W Hackborn, "Asymmetric Stokes flow between parallel planes due to a rotlet," *Journal of Fluid Mechanics* **218**, 531–546 (1990).
- [38] H K Moffatt, "Viscous and resistive eddies near a sharp

- corner,” *Journal of Fluid Mechanics* **18**, 1–18 (1964).
- [39] George Haller, “Lagrangian coherent structures,” *Annual Review of Fluid Mechanics* **47**, 137–162 (2015).
- [40] M Sudharsan, Steven L Brunton, and James J Riley, “Lagrangian coherent structures and inertial particle dynamics,” *Physical Review E* **93**, 033108 (2016).
- [41] R U I Ni, Nicholas T Ouellette, and Greg A Voth, “Alignment of vorticity and rods with Lagrangian fluid stretching in turbulence,” *Journal of Fluid Mechanics* **743** (2014), arXiv:arXiv:1311.0739v1.
- [42] Erik van Sebille, Matthew H England, and Gary Froyland, “Origin, dynamics and evolution of ocean garbage patches from observed surface drifters,” *Environmental Research Letters* **7**, 44040 (2012).
- [43] Yang Ding and Eva Kanso, “Selective particle capture by asynchronously beating cilia,” *Physics of Fluids* **27**, 121902 (2015).